Influence of hydrogen bonds and temperature on dielectric properties

Jordi Ortiz de Urbina and Gemma Sesé*

Departament de Física, Universitat Politècnica de Catalunya, Campus Nord-Mòdul B4, c/ Jordi Girona 1-3, 08034 Barcelona, Spain

(Received 29 January 2016; revised manuscript received 2 June 2016; published 6 July 2016)

Dielectric properties are evaluated by means of molecular dynamics simulations on two model systems made up of dipolar molecules. One of them mimics methanol, whereas the other differs from the former only in the ability to form hydrogen bonds. Static dielectric properties such as the permittivity and the Kirkwood factor are evaluated, and results are analyzed by considering the distribution of relative orientations between molecular dipoles. Dipole moment–time correlation functions are also evaluated. The relevance of contributions associated with autocorrelations of molecular dipoles and with cross-correlations between dipoles belonging to different molecules has been investigated. For methanol, the Debye approximation for the overall dipole moment correlation function is not valid at room temperature. The model applies when hydrogen bonds are suppressed, but it fails upon cooling the nonassociated liquid. Important differences between relaxation times associated with dipole auto- versus cross-correlations as well as their relative relevance are at the root of the Debye model breakdown.

DOI: 10.1103/PhysRevE.94.012605

I. INTRODUCTION

The search for the microscopic mechanisms governing the dielectric response in polar liquids is a topic of fundamental interest. To this end, experimental measurements on slightly different materials can be performed and the effect of such differences on the measured properties can be analyzed. Dielectric spectroscopy has been used, for example, to elucidate how the molecular structure of polar compounds influences their response to external electric fields and, also, how this response changes at temperatures approaching the glass transition [1]. Generally speaking, results emphasize the relevance of intermolecular interactions in governing relaxation dynamics.

Because of their role in many chemical processes, hydrogen-bonded (HB) liquids have attracted much attention. Several features characterizing their dielectric behavior have been attributed to the properties of their corresponding HB networks [2–5]. Among HB liquids, relaxation in monoalcohols has been investigated using a variety of experimental techniques. It is generally accepted that their dielectric spectra show three processes. Nevertheless, they are material dependent, and the conditions under which the structural and the secondary peak merge, as well as the nature of the third Debye peak, are still under debate [6,7]. In addition, study of the microscopic mechanisms governing their macroscopic dielectric properties can help us to advance the understanding of systems with more complicated HB structures.

Computer simulation is a complementary technique that can be used to unveil the signatures of molecular model details onto macroscopic properties. Large samples and long simulations are required in order to obtain statistically significant results for the dielectric properties, which are collective in nature. For low molecular weight liquids, it was shown that samples of a few hundreds of particles behave like macroscopic dielectric materials [8,9]. Simplified molecular models have been considered in computational studies of liquids because they allow simulations to span larger time intervals. Then united atom models have been used to evaluate dielectric properties in alcohols like methanol [10,11] and ethanol [12] at room temperature using molecular dynamics simulations.

The purpose of our work is twofold. On the one hand, we intend to use simulations to get some insight into the influence of HB on the dielectric properties of a methanol model (MeOH) at room temperature. Both static and dynamic properties are obtained for MeOH and for an ideal methanol-like system whose molecules have the same dipolar moment as do those in MeOH but that lack sites for hydrogen bonding. It should be noted that 99% of MeOH molecules are HB at room temperature [13]. The effect of HB on ionic association [14], single-particle dynamics [15–17], and thermodynamic properties [18] was previously investigated in this system. On the other hand, the influence of temperature on the dielectric properties of the nonassociated liquid at very low temperatures is also studied. It has been reported that systems composed of Lennard-Jones rigid asymmetric diatomic molecules exhibit both structural and secondary relaxation processes in rotation below the onset temperature [19,20]. We intend to examine the dielectric relaxation behavior of a system made up of slightly asymmetric diatomic molecules, with an added constant dipole moment. Results are also tested against existing theoretical models.

The paper is organized as follows. In Sec. II, simulation details and computed correlation functions are presented. Results of static and dynamic dielectric properties are reported in Sec. III and are also tested against existing theoretical models. Some concluding remarks are gathered in Sec. IV.

II. MODELS AND METHODOLOGY

Molecular dynamics simulations of a system that mimicks MeOH have been performed. A three-site rigid molecular model has been used. Molecular sites belonging to different molecules interact by means of electrostatic and Lennard-Jones forces according to the optimized potential for liquid simulations [21]. The Ewald summation [22] has been used in the evaluation of electrostatic interactions. A system composed

*gemma.sese@upc.edu

TABLE I. Parameters for the Lennard-Jones potentials used in molecular dynamics simulations of MeOH and MeO. Electric charges for their sites are also listed.

			$q(e)$	
Site	σ (Å)	ϵ (kcal/mol)	MeOH	MeO
O	3.071	0.170	−0.700	−0.323
H	0.0	0.0	0.435	
Me	3.775	0.207	0.265	0.323

of rigid diatomic neutral molecules has also been simulated (metoxi; MeO). The model is similar to the one considered for MeOH but hydrogen sites have been suppressed so that HB cannot be established. Two interacting sites per molecule have been considered and short-range Lennard-Jones interactions are coincident with those used for the MeOH sample. Their masses are those of oxygen and of the methyl group, respectively. They have been assigned charges such that the molecular dipole moment equals that of MeOH molecules (2.22 D) [15]. Potential parameters are listed in Table I.

Simulated samples are made up of $N = 1000$ molecules located in a cubic box with periodic boundary conditions. After being equilibrated at room temperature, the MeO system has been quenched at constant pressure according to the procedure described in [16]. For 10 selected temperatures between 298 and 123 K, the samples have been equilibrated. Production runs of 1 ns at the highest temperature and of 6 ns at the lowest temperature have been performed in the (N,V,T) ensemble. The computed glass transition temperature for MeO is 95 K [17].

Correlation functions of the system's dipole density have been obtained in order to study the dielectric properties. They involve longitudinal $[\vec{M}_L(\vec{k},t)]$ and transverse $[\vec{M}_T(\vec{k},t)]$ Fourier components of the dipole density, which are defined as

$$\vec{M}_L(\vec{k},t) = \sum_{j=0}^{N} \hat{k}\hat{k} \cdot \vec{\mu}_j(t) \exp[i\vec{k} \cdot \vec{r}_j(t)], \tag{1}$$

$$\vec{M}_T(\vec{k},t) = \sum_{j=0}^{N} (1 - \hat{k}\hat{k}) \cdot \vec{\mu}_j(t) \exp[i\vec{k} \cdot \vec{r}_j(t)], \tag{2}$$

where $\vec{\mu}_j$ is the dipole moment of molecule j, and $\vec{r}_j(t)$ is the position of the molecule's center of mass. $\vec{k}$ should be compatible with the box length L; specifically, $\vec{k} = 2\pi/L(l,m,n)$, where L is the box length, l, m, and n are integers, and $\hat{k}$ is the corresponding unit vector. Their correlations have been evaluated according to

$$\Phi_A(\vec{k},t) = \langle \vec{M}_A(\vec{k},t) \cdot \vec{M}_A(-\vec{k},0) \rangle / \langle |\vec{M}_A(\vec{k},0)|^2 \rangle, \tag{3}$$

where A can refer to the longitudinal (L) component or to the transverse (T) component. By means of the linear response theory it is possible to relate the components of the susceptibility tensor $\chi_A^0(\vec{k},w)$ to $\Phi_A(\vec{k},t)$ for a system of rigid and nonpolarizable molecules through [23]

$$\chi_A^0(\vec{k},w) = [1 + i\,w\Phi_A(\vec{k},w)] \langle |\vec{M}_A(\vec{k},0)|^2 \rangle / (\nu_A L^3 k_b T \varepsilon), \tag{4}$$

with $\nu_L = 1$ and $\nu_T = 2$, and

$$\Phi_A(\vec{k},w) = \int_0^\infty dt\, \Phi_A(\vec{k},t) \exp(i\,wt). \tag{5}$$

Then the longitudinal $[\varepsilon_L(\vec{k},w)]$ and transverse $[\varepsilon_T(\vec{k},w)]$ components of the dielectric permittivity tensor are

$$\frac{\varepsilon_L(\vec{k},w) - 1}{\varepsilon_L(\vec{k},w)} = \chi_L^0(\vec{k},w), \tag{6}$$

$$\varepsilon_T(\vec{k},w) - 1 = \chi_T^0(\vec{k},w). \tag{7}$$

For the static case $(w = 0)$ and for an isotropic system, it is possible to write, using that $y = \frac{4\pi}{9}\rho\mu^2/(k_B t)$,

$$\frac{\varepsilon_L(k) - 1}{\varepsilon_L(k)} = y \frac{\langle |\vec{M}_L(k,0)|^2 \rangle}{N\mu^2}, \tag{8}$$

$$\varepsilon_T(k) - 1 = y \frac{\langle |\vec{M}_T(k,0)|^2 \rangle}{2N\mu^2}. \tag{9}$$

For a large enough system, that is, when k is sufficiently small,

$$\lim_{k\to 0} \varepsilon_L(k) \approx \lim_{k\to 0} \varepsilon_T(k) \approx \varepsilon, \tag{10}$$

ε being the dielectric permittivity of the system, which can also be evaluated in a system of nonpolarizable molecules by using [24]

$$\epsilon = 1 + \tfrac{4}{3}\pi\rho\beta\mu^2 g, \tag{11}$$

where ρ is the molecular density, $\beta = 1/(k_B T)$, and μ is the molecular dipole moment modulus. g is the finite-system Kirkwood factor, which can be evaluated in simulations by means of [8,25]

$$g = \frac{\left(\sum_i \vec{\mu}_i\right)^2}{N\mu^2}. \tag{12}$$

For a system of orientationally uncorrelated dipoles, $g = 1$. If the dipoles tend to be parallel, $g > 1$. Otherwise, $g < 1$. Using Kirkwood's formula [26,27], the Kirkwood factor for an infinite system can be calculated as

$$g^0 = g\frac{(2\epsilon + 1)}{3\epsilon}. \tag{13}$$

It is also possible to evaluate the frequency-dependent permittivity $[\varepsilon(\omega)]$ from the total dipole moment correlation function,

$$\Phi(t) = \frac{\langle \vec{M}(0) \cdot \vec{M}(t) \rangle}{\langle |\vec{M}(0)|^2 \rangle}, \tag{14}$$

where $\vec{M}(t)$ is the dipole moment of the sample at time t, which is related to the individual molecular dipole moments $\vec{M}(t) = \sum_i^N \vec{\mu}_i(t)$. The real and imaginary components of $\varepsilon(\omega)$ are, respectively [28],

$$\varepsilon'(w) = \varepsilon - (\varepsilon - 1)\omega \int_0^\infty \Phi(t) \sin(wt) dt, \tag{15}$$

$$\varepsilon''(w) = (\varepsilon - 1)\omega \int_0^\infty \Phi(t) \cos(wt) dt. \tag{16}$$

TABLE II. Kirkwood factor (g) and dielectric permittivity (ϵ) evaluated using Eqs. (12) and (11), respectively, from simulations of methanol (MeOH) and metoxi (MeO) at several temperatures. Kirkwood factor values corrected according to Eq. (13) are also listed (g^0). Uncertainties were estimated from statistical fluctuations.

T (K)	$g \pm \sigma_g$	$\epsilon \pm \sigma_\epsilon$	$g^0 \pm \sigma_{g^0}$
	MeOH		
298	2.5 ± 0.2	20 ± 2	1.7 ± 0.2
	MeO		
298	1.9 ± 0.1	15 ± 1	1.3 ± 0.1
268	2.0 ± 0.1	16 ± 1	1.6 ± 0.1
238	2.2 ± 0.1	23 ± 1	1.6 ± 0.1
218	2.3 ± 0.1	25 ± 1	1.6 ± 0.1
208	2.5 ± 0.1	30 ± 1	1.6 ± 0.1
198	2.5 ± 0.1	33 ± 1	1.7 ± 0.1
178	2.6 ± 0.1	39 ± 1	1.8 ± 0.1
158	3.1 ± 0.1	51 ± 1	2.0 ± 0.1
138	3.9 ± 0.1	74 ± 1	2.0 ± 0.1
123	3.4 ± 0.1	75 ± 2	2.3 ± 0.2

III. RESULTS

A. Static dielectric properties

The finite-system Kirkwood factor has been evaluated in our simulations by means of Eq. (12). Its values are listed in Table II, as well as those of the permittivity and the infinite-system Kirkwood factor, which have been obtained using Eqs. (11) and (13), respectively. The evaluated permittivity for MeOH is 20, which is significantly lower than the experimental value obtained for methanol (32) [29]. This is the consequence of the approximations in the model such as the neglect of the polarizability and the use of united-atom sites. It is in reasonable agreement with previous work [10] that considered the same approximations with slightly different potential parameters.

It is apparent from the results in Table II that suppressing hydrogen bonding results in smaller values for the Kirkwood factors and, consequently, for the permittivity. They are about 25% lower than those obtained for MeOH. This is consistent with the fact that, even though the molecular dipole is the same for both systems, the proportion of electrostatic energy is larger in the system with HB [30]. In the latter, electrostatic interactions are highly directional, whereas they tend to be isotropic in the nonassociated system.

Upon cooling, the Kirkwood factors and the permittivity of MeO increase. Taking into account that the modulus of the molecular dipole moment is constant, this behavior should be related to an increase in correlations between the orientations of dipole moments belonging to different molecules, as subsequently discussed.

The function $\langle\cos(\theta(r))\rangle$, θ being the angle between the dipole moments of two molecules whose centers of mass are separated by a distance r, is displayed in the inset in Fig. 1. At room temperature, it is apparent that orientational correlations between dipole moments belonging to different molecules rapidly decrease with distance and that the contribution of the first shell is the most important in both systems. It is also shown that MeOH molecules located within the first shell of a given one tend to align their molecular moments. This restricted orientation between dipoles is retained at larger distances, which is consistent with a linear HB network. This is not true for the nonassociated system, where orientation tends to be antiparallel for the closest molecules, but a parallel orientation is also possible within the first shell. In this case, Kirkwood factors result from the addition of positive (parallel) and negative (antiparallel) terms, which leads to smaller values than those obtained for methanol.

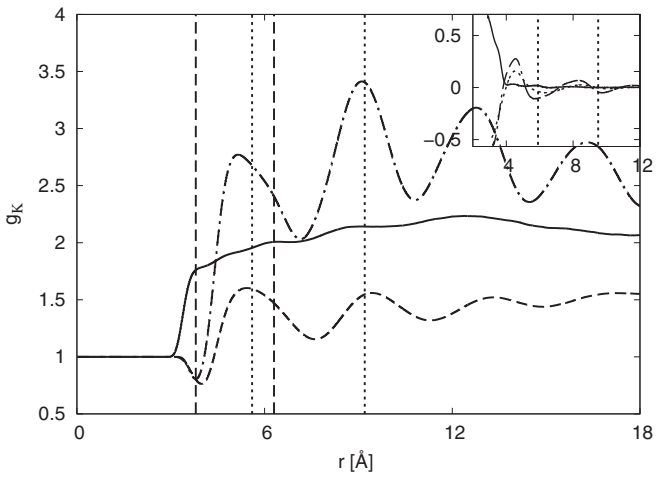

FIG. 1. Distance-dependent Kirkwood factor $g_\kappa(r)$ evaluated according to Eq. (17) for MeOH (solid line) and MeO (dashed line) at 298 K and for MeO at 123 K (dashed-dotted line). Vertical lines are drawn at limiting distances of the first and second shell of MeOH (dashed lines) and MeO (dotted lines). Inset: $\langle\cos(\theta(r))\rangle$ for the same systems, θ being the angle between dipole moments of two molecules whose centers of mass are separated by a distance r. Limiting distances of the first and second shells of MeO are also shown (dotted vertical lines).

The behavior of $\langle\cos(\theta(r))\rangle$ for the nonassociated system does not qualitatively change upon cooling, as occurs for most pair distribution functions [30]. It is apparent in Fig. 1, however, that orientational correlations tend to increase not just between molecules within the first coordination shell. Moreover, the relevance of correlations with molecules in the second shell increases significantly at low temperatures.

The dependence of the Kirkwood factor with r has been analyzed by means of [8]

$$g_\kappa(r) = 1 + 4\pi\rho \int_0^r g(r)\langle\cos(\theta(r))\rangle r^2 dr, \qquad (17)$$

where $g(r)$ is the radial distribution function for molecular centers of mass. $g_\kappa(r)$ functions are displayed in Fig. 1. At room temperature, the results for MeOH are qualitatively different from those for MeO. Whereas restrictions in the orientation of MeOH molecules prevent the function from oscillating as the integral is extended to larger distances, marked oscillations are apparent in the nonassociated system. These oscillations become more important upon cooling of the system. In addition, it is apparent that the contribution of dipoles located in the second solvation shell to $g_\kappa(r)$ experiences the largest increase as the temperature decreases.

TABLE III. Longitudinal and transverse components of the wave-vector-dependent static constant for methanol (up) and metoxi at 298 K (middle) and at 123 K (down).

$(k/k_{\min})^2$	k (Å^{-1})	$\langle\lvert\vec{M}_L(\vec{k},0)\rvert^2\rangle/N\mu^2$	$\langle\lvert\vec{M}_T(\vec{k},0)\rvert^2\rangle/2N\mu^2$	$\varepsilon_L(k)$	$\varepsilon_T(k)$
1	0.1542	0.0217 ± 0.001	0.95 ± 0.21	0.468 ± 0.078	20.22 ± 4.63
2	0.2180	0.0212 ± 0.001	0.92 ± 0.16	0.473 ± 0.063	19.71 ± 3.40
3	0.2671	0.0209 ± 0.001	0.88 ± 0.14	0.482 ± 0.061	19.6 ± 2.88
1	0.1542	0.0215 ± 0.0004	0.64 ± 0.04	0.477 ± 0.032	15.07 ± 0.857
2	0.2180	0.0218 ± 0.0002	0.63 ± 0.02	0.484 ± 0.020	13.81 ± 0.418
3	0.2671	0.0223 ± 0.0002	0.62 ± 0.02	0.502 ± 0.021	12.87 ± 0.344
1	0.1635	0.0080 ± 0.0002	1.26 ± 0.25	0.511 ± 0.041	82.3 ± 16.3
2	0.2313	0.0081 ± 0.0002	1.28 ± 0.11	0.484 ± 0.043	81.6 ± 6.9
3	0.2833	0.0082 ± 0.0002	1.13 ± 0.13	0.502 ± 0.042	77.1 ± 8.41

Values for the longitudinal and transverse components of the wave-vector static permittivity constant, defined in Eqs. (8) and (9), respectively, are listed in Table III. For all systems, Eq. (10) is fulfilled for the transverse component, which proves that the simulated samples are big enough so that the results can be considered representative of a macroscopic isotropic fluid. Discrepancies observed for the longitudinal component can be attributed to the fact that, according to Eq. (8), $\varepsilon_L(k)$ displays a singularity for $y = (N\mu^2)/(|\vec{M}_L(k,0)|^2)$, which is numerically very close to the y values obtained for our systems [10].

B. Dynamic dielectric properties

The total dipole moment correlation function $\Phi(t)$, defined in (14), can be decomposed into self and distinct contributions according to

$$\Phi(t) = \frac{N\mu^2}{\langle|\vec{M}(0)|^2\rangle}\Phi_s(t) + \frac{N(N-1)\langle\vec{\mu}_i(0)\cdot\vec{\mu}_j(0)\rangle}{\langle|\vec{M}(0)|^2\rangle}\Phi_d(t), \tag{18}$$

where $\Phi_s(t)$ is the self-correlation function of individual dipoles and $\Phi_d(t)$ is the cross-correlation function between dipoles corresponding to different molecules,

$$\Phi_s(t) = \frac{\langle\vec{\mu}_i(t)\cdot\vec{\mu}_i(0)\rangle}{\langle|\vec{\mu}_i(0)|^2\rangle}, \tag{19}$$

$$\Phi_d(t) = \frac{\langle\vec{\mu}_i(t)\cdot\vec{\mu}_j(0)\rangle}{\langle\vec{\mu}_i(0)\cdot\vec{\mu}_j(0)\rangle}, \tag{20}$$

with $i \neq j$. The finite-system Kirkwood factor defined in Eq. (12) can also be evaluated as

$$g = 1 + (N-1)\langle\vec{\mu}_i(0)\cdot\vec{\mu}_j(0)\rangle/\mu^2, \tag{21}$$

which leads to the following more compact expression for $\Phi(t)$:

$$\Phi(t) = \frac{1}{g}\Phi_s(t) + \left(1 - \frac{1}{g}\right)\Phi_d(t). \tag{22}$$

Results for $\Phi(t)$ at room temperature are displayed in Fig. 2. On a short time scale, some oscillations appear in MeOH but not in the nonassociated system. A similar behavior is apparent in $\Phi_s(t)$. They are probably a signature of the librational dynamics associated with the existence of hydrogen bonds, as suggested in previous simulations of ethanol [12]. The long time decay of both functions cannot be properly modeled by exponentials, and they are best fit with stretched exponential functions [$\Phi_s(t) = A\exp(-(t/\tau_1)^{\beta_1})$ and $\Phi(t) = A\exp(-(t/\tau_\Phi)^{\beta_\Phi})$, respectively]. Exponent values and relaxation times are listed in Table IV. It is remarkable that τ_Φ takes the same value as the hydrogen-bond lifetime in MeOH [31], which confirms that it is the breaking of a hydrogen bond that makes possible the orientation of the liberated dipoles, as previously suggested [32]. As reported in Table IV, $\tau_\Phi > \tau_1$ in MeOH, whereas $\tau_\Phi \approx \tau_1$ when HB is suppressed. For the latter system, both $\Phi_s(t)$ and $\Phi(t)$ display the same qualitative behavior: fast initial decays followed by exponential-like long-time relaxation periods, much shorter than those observed for the HB liquid.

Upon cooling of the MeO system, the exponential long-time decay becomes a stretched exponential, even though the exponent never takes values smaller than 0.8 at the analyzed temperatures. It is apparent in Table IV that relaxation times increase upon cooling and that the times for $\Phi(t)$ are longer than those obtained for $\Phi_s(t)$ at all temperatures. Moreover, differences between them increase as the temperature decreases, suggesting that cross-correlations become more important.

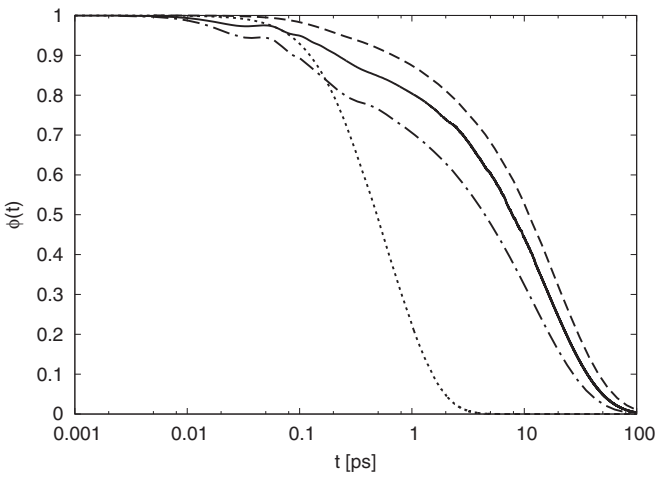

FIG. 2. Total dipole moment correlation function [$\Phi(t)$] for MeOH (solid line) and MeO (dotted line) at 298 K, and for MeO at 123 K (dashed line). Also shown is the self-autocorrelation function of individual dipoles [$\Phi_s(t)$] for MeOH at 298 K (dashed-dotted line).

TABLE IV. Parameters associated with stretched exponential fits of the self $[\Phi_s(t)]$ dipole correlation functions (τ_1 and β_1) and of the total $[\Phi(t)]$ dipole correlation functions (τ_ϕ and β_ϕ). Estimated errors for the stretched exponents are 5%.

T (K)	$\tau_1 \pm \sigma_{\tau_1}$	β_1	$\tau_\phi \pm \sigma_{\tau_\phi}$	β_ϕ
		MeOH		
298	11.8 ± 0.3	0.85	16 ± 10	0.9
		MeO		
298	0.62 ± 0.02	1	0.64 ± 0.10	1
268	0.80 ± 0.04	1	0.86 ± 0.02	1
238	1.10 ± 0.02	1	1.14 ± 0.12	1
218	1.14 ± 0.03	0.9	1.51 ± 0.30	0.9
208	1.34 ± 0.04	0.9	1.98 ± 0.20	1
198	1.60 ± 0.05	0.9	2.16 ± 0.36	0.85
178	2.26 ± 0.03	0.9	3.30 ± 0.26	0.9
158	3.42 ± 0.06	0.85	5.06 ± 0.74	0.9
138	7.08 ± 0.33	0.85	13.2 ± 3.1	0.8
123	13.8 ± 1.3	0.8	19.0 ± 5.8	0.9

The Debye model considers a liquid as a viscous continuum in which the dispersed molecules perform isotropic Brownian reorientations. Then it states that $\Phi(t)$ displays an exponential long-time decay which can be approximated by the single-molecule reorientation function $\Phi_s(t)$ [33]. From our results, MeOH appears as a non-Debye fluid at room temperature. On the contrary, MeO is a Debye fluid at high temperatures, but a breakdown of the Debye model occurs at low temperatures. It is interesting to analyze the relative contribution of cross-correlations to the overall $\Phi(t)$ function. Results are listed in Fig. 3. At room temperature, the contribution of cross-correlations to $\Phi(t)$ for MeOH is about 60%, whereas in the nonassociated system, it is about 45%. For the nonassociated system, the Debye model is valid at the higher analyzed temperatures not because cross-correlations are unimportant but because their associated relaxation times are similar to

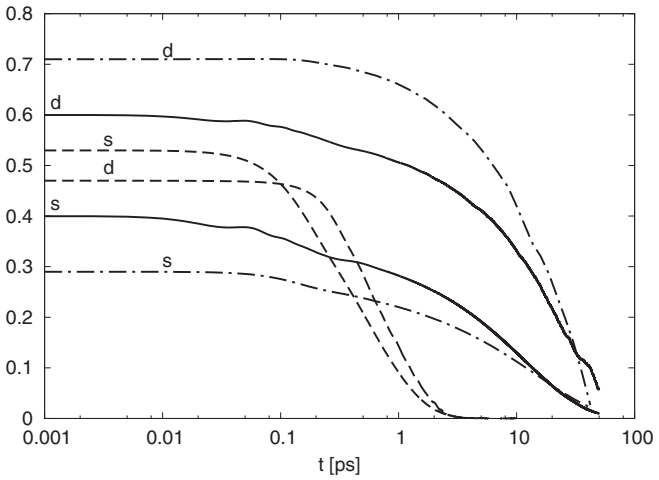

FIG. 3. Self (s), $\frac{1}{g}\Phi_s(t)$, and distinct (d), $(1-\frac{1}{g})\Phi_d(t)$, contributions to the total dipole moment correlation functions for MeOH (solid lines) and MeO (dashed lines) at 298 K and for MeO at 123 K (dashed-dotted lines).

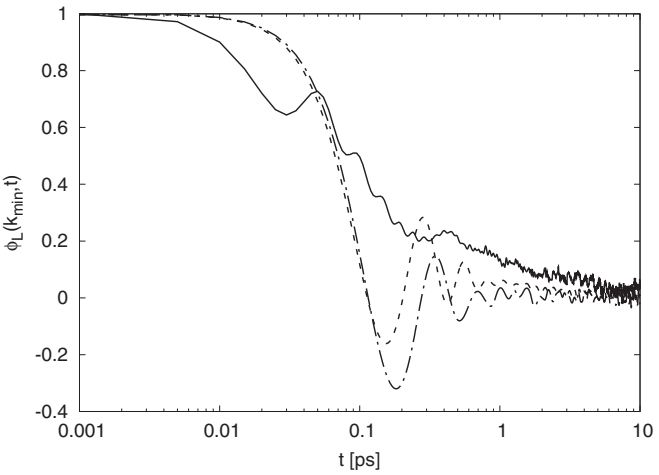

FIG. 4. $\Phi_L(\vec{k},t)$ with $k = k_{\min} = 2\pi/L$ for MeOH (solid line) and MeO (dashed-dotted line) at 298 K and for MeO at 123 K (dashed line).

those for self-correlations. Upon cooling of the system, the relevance of the cross-correlation term increases significantly, up to 70% at the lowest analyzed temperature, as shown in Fig. 3. Then both the increase in the relative relevance of cross-correlations and the increase in the difference between the time scale of self- and that of cross-correlations are at the root of the Debye model breakdown.

$\Phi_T(\vec{k},t)$ and $\Phi_L(\vec{k},t)$, defined by Eq. (3), have also been calculated. The three smallest possible values for k have been considered, and a very mild dependence on k has been obtained over this range. It has been found that the transverse function $\Phi_T(\vec{k},t)$ is very similar to $\Phi(t)$ for all systems. Longitudinal functions $\Phi_L(\vec{k},t)$ are very short-lived in all cases, as shown in Fig. 4. In addition, a fast oscillatory decay is obtained for MeOH, whereas the initially monotonically decreasing function is followed by pronounced overdamped oscillations in the nonassociated system. Thus, suppression of HB modifies, even qualitatively, the initial decay of $\Phi_L(\vec{k},t)$. Decreasing the temperature does not affect the initial decay of the function, as shown in Fig. 4.

Within the theoretical framework of the Debye model, the components of the frequency-dependent permittivity, defined by Eqs. (15) and (16), can be approximated by

$$\varepsilon'(w) - 1 = \frac{\varepsilon - 1}{1 + w^2\tau_1^2}, \tag{23}$$

$$\varepsilon''(w) = \frac{(\varepsilon - 1)w\tau_1}{1 + w^2\tau_1^2}. \tag{24}$$

Recalling that $\varepsilon(w) = \varepsilon'(w) - i\varepsilon''(w)$, they can be merged into

$$\frac{\varepsilon(w) - 1}{\varepsilon - 1} = \frac{1}{1 + iw\tau_1}. \tag{25}$$

Davidson-Cole modified Eq. (25) by adding a parameter β [34],

$$\frac{\varepsilon(w) - 1}{\varepsilon - 1} = \frac{1}{(1 + iw\tau)^\beta}, \tag{26}$$

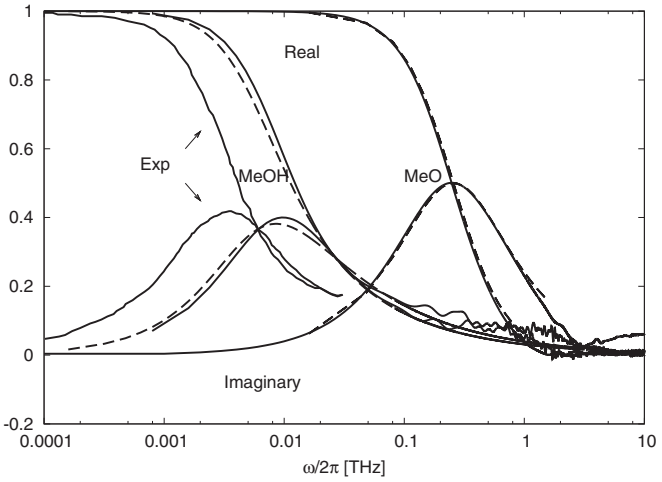

FIG. 5. Real $[(\varepsilon'(w)-1)/(\varepsilon-1)]$ and imaginary $[\varepsilon''(w)/(\varepsilon-1)]$ normalized components of the frequency-dependent permittivity for MeOH and MeO (solid lines) at 298 K. The Davidson-Cole approach for MeOH (dashed lines), Debye approximation for MeO (dashed lines), and experimental (Exp) results for methanol (solid lines) [29] are also shown.

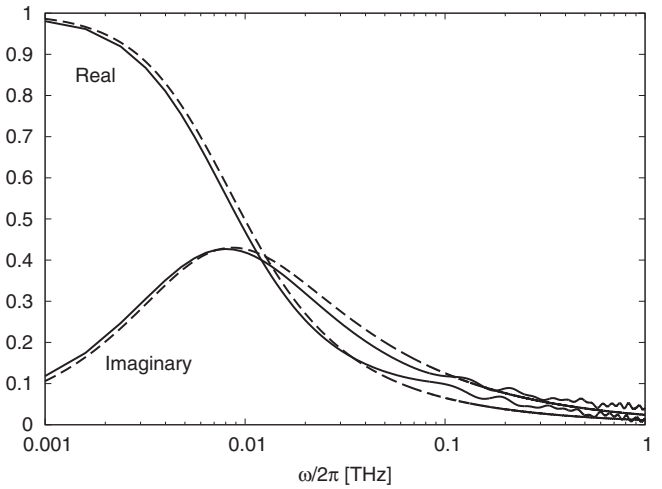

FIG. 6. Real $[(\varepsilon'(w)-1)/(\varepsilon-1)]$ and imaginary $[\varepsilon''(w)/(\varepsilon-1)]$ normalized components of the frequency-dependent permittivity for MeO at 123 K (solid lines). The Davidson-Cole approach is also shown (dashed lines).

where $0 < \beta \leqslant 1$. Using that $\tan(\phi) = w\tau$,

$$\frac{1}{(1+iw\tau)^{\beta}} = \frac{1}{\left(1+i\frac{\sin(\phi)}{\cos(\phi)}\right)^{\beta}} = [\cos^{\beta}(\phi)e^{-i\phi\beta}], \tag{27}$$

$$\varepsilon' = \cos^{\beta}(\phi)\cos(\beta\phi), \tag{28}$$

$$\varepsilon'' = \cos^{\beta}(\phi)\sin(\beta\phi). \tag{29}$$

Real and imaginary components of the frequency-dependent permittivity at room temperature are displayed in Fig. 5, as well as recent experimental measurements for methanol [29]. In order to leave aside the discrepancies observed for the static permittivity, the functions $(\varepsilon'(w)-1)/(\varepsilon-1)$ and $\varepsilon''(w)/(\varepsilon-1)$ are plotted. Calculations on MeOH qualitatively reproduce experimental results. According to them, one main peak is apparent at the imaginary component of the permittivity. Some quantitative discrepancies arise in the time scale of the real component and in the peak frequency of the imaginary component. It is apparent that functions obtained in simulations are shifted towards higher frequencies compared with experiment. Similar behavior was observed for a four-site model with rigid bonds of ethanol [12]. The neglect of polarizability is probably at the root of these discrepancies, as previously argued [11]. Additionally, the coarse-grained nature of the molecular model might also be a relevant factor. Fast vibrational motions, suppressed by coarse graining, might hinder molecular relaxation, resulting in longer experimental relaxation times. Fits of the simulation results to the Davidson-Cole equations, (28) and (29), are also displayed in Fig. 5, and a reasonable agreement has been obtained.

Suppression of hydrogen bonding produces shifts of the real and imaginary components of the frequency-dependent permittivity towards higher frequencies. Upon cooling, both components shift towards lower frequencies, and they intersect at frequencies higher than the one corresponding to the imaginary component peak. It is apparent in Fig. 5 that the Debye model is a very good approximation for the nonassociated system at room temperature. Upon cooling of the system, only one primary relaxation process is detected, similar to the results obtained for slightly asymmetric Lennard-Jones molecules [20]. The Debye model is less satisfactory at low temperatures, and the Davidson-Cole approach, shown in Fig. 6, produces better results. This is consistent with the emerging dynamic heterogeneities in the system [35].

IV. CONCLUDING REMARKS

Dielectric properties have been computed in two model systems which differ only in their ability to establish hydrogen bonds. One of them mimicks methanol. It has been obtained that the Kirkwood factor and, consequently, the permittivity decrease significantly when hydrogen bonding is suppressed. The Kirkwood factor is larger in methanol as a consequence of the more restricted relative orientations between molecular dipoles. Specifically, methanol molecules located within the first shell of a given one tend to align their molecular dipoles, whereas both parallel and antiparallel orientations are allowed in the nonassociated system. Upon cooling of this liquid, the Kirkwood factor also increases, and the contribution of dipoles located within the second solvation shell experiences the largest increase.

In analyses of the dipole correlation function for the nonassociated liquid at ambient temperature, it has been found that the contribution of dipole autocorrelations is slightly more important than that of correlations between dipoles belonging to different molecules. Conversely, correlations between orientations of different molecules are more relevant in methanol. In addition, relaxation times associated with the self and the distinct parts differ significantly, whereas they are quite similar in the system without hydrogen bonds. Consequently, the Debye model reproduces the long-time regime of the nonassociated system but not that of methanol at room temperature. For very low temperatures, relaxation in

the nonassociated liquid cannot be reproduced by the Debye model. The Debye breakdown takes place not only because the relative relevance of cross-correlations increases but also because differences between self- and cross-correlation time scales increase. In addition, it has been confirmed for methanol that relaxation of the overall dipole correlation function is associated with the breaking of hydrogen bonds.

The wave-vector dependence of the dipole density–time correlation function has also been studied. This function has been split into its transverse and its longitudinal parts. The behavior of the transverse component is very similar to that of the overall dipole-time correlation function. The longitudinal component relaxes considerably more rapidly than the transverse part in both systems. Librations appearing at short times in methanol disappear when hydrogen bonds are removed, and the function displays an overdamped oscillatory behavior.

ACKNOWLEDGMENT

Financial support by MINECO (Project No. FIS2012-39443-C02-01) is acknowledged.

[1] Z. Chen, D. Bi, R. Liu, Y. Tian, L.-M. Wang, and K. L. Ngai, Chem. Phys. Lett. **551**, 81 (2012).
[2] L.-M. Wang and R. Richert, J. Chem. Phys. **121**, 11170 (2004).
[3] B. D. Watode, P. G. Hudge, and A. C. Kumbharkhane, J. Mol. Liq. **198**, 51 (2014).
[4] V. Conti Nibali and M. Havenith, J. Am. Chem. Soc. **136**, 12800 (2014).
[5] H. A. Chaube, V. A. Rana, P. Hudge, and A. C. Kumbharkhane, J. Mol. Liq. **193**, 29 (2014).
[6] D. Fragiadakis, C. M. Roland, and R. Casalini, J. Chem. Phys. **132**, 144505 (2010).
[7] R. Böhmer, C. Gainaru, and R. Richert, Phys. Rep. **545**, 125 (2014).
[8] M. Neumann, O. Steinhauser, and G. S. Pawley, Mol. Phys. **52**, 97 (1984).
[9] D. M. F. Edwards, P. A. Madden, and I. R. McDonald, Mol. Phys. **51**, 1141 (1984).
[10] T. Fonseca and B. M. Ladanyi, J. Chem. Phys. **93**, 8148 (1990).
[11] M. S. Skaf, T. Fonseca, and B. M. Ladanyi, J. Chem. Phys. **98**, 8929 (1993).
[12] L. Saiz, E. Guàrdia, and J. A. Padró, J. Chem. Phys. **113**, 2814 (2000).
[13] R. Palomar and G. Sesé, J. Chem. Phys. **133**, 044501 (2010).
[14] F. Hirata and R. M. Levy, J. Phys. Chem. **91**, 4788 (1987).
[15] E. Guàrdia, G. Sesé, and J. A. Padró, J. Mol. Liq. **62**, 1 (1994).
[16] R. Palomar and G. Sesé, J. Phys. Chem. B **109**, 499 (2005).
[17] G. Sesé, J. Ortiz de Urbina, and R. Palomar, J. Chem. Phys. **137**, 114502 (2012).
[18] D. Fragiadakis and C. M. Roland, J. Chem. Phys. **138**, 12A502 (2013).
[19] D. Fragiadakis and C. M. Roland, Phys. Rev. E **89**, 052304 (2014).
[20] D. Fragiadakis and C. M. Roland, Phys. Rev. E **91**, 022310 (2015).
[21] W. L. Jorgensen, J. Phys. Chem. **90**, 1276 (1986).
[22] M. P. Allen and D. J. Tildesley, *Computer Simulations of Liquids* (Clarendon Press, Oxford, UK, 1987).
[23] P. A. Madden and D. Kivelson, Adv. Chem. Phys. **LVI**, 467 (1984).
[24] D. Frenkel and B. Smit, *Understanding Molecular Simulation. From Algorithms to Applications* (Academic Press, San Diego, CA, 2002).
[25] M. Neumann, J. Chem. Phys. **82**, 5663 (1985).
[26] J. G. Kirkwood, J. Chem. Phys. **7**, 911 (1939).
[27] S. W. de Leeuw, J. W. Perram, and E. H. Smith, Annu. Rev. Phys. Chem. **37**, 245 (1986).
[28] D. Levesque, J.-J. Weis, and D. Oxtoby, J. Chem. Phys. **79**, 917 (1983).
[29] H. A. Chaube, V. A. Rana, P. Hudge, and A. C. Kumbharkhane, J. Mol. Liq. **211**, 346 (2015).
[30] R. Palomar, Ph.D. thesis, Technical University of Catalonia (2007); http://www.tdx.cat/handle/10803/6589.
[31] J. A. Padró, L. Saiz, and E. Guàrdia, J. Mol. Struct. **416**, 243 (1997).
[32] C. Brot and M. Magat, J. Chem. Phys. **39**, 841 (1963).
[33] D. A. McQuarrie, *Statistical Mechanics* (University Science Books, Herndon, VA, 2000).
[34] D. W. Davidson and R. H. Cole, J. Chem. Phys. **18**, 1417 (1950).
[35] R. Palomar and G. Sesé, Phys. Rev. E **75**, 011505 (2007).